Electronic Supplementary Information

Efficient and Stable Perovskite Solar Cells Based on a Quasi-Point-Contact and Rear-Reflection Structure with 22.5% Efficiency

Jinpeng Wu[a,b], Yanyan Fang[a,b], Di Zhang[a,b], Sidong Zhang[a,b], Jing Wan[a,b], Rui Wen[a,b], Xiaowen Zhou[a,b], Nianqing Fu[c], and Yuan Lin[a,b]**

[a] CAS Key Laboratory of Photochemistry, CAS Research/Education Center for Excellence in Molecular Sciences, Beijing National Laboratory for Molecular Sciences (BNLMS), Institute of Chemistry, Chinese Academy of Sciences (CAS)

Beijing 100190, P. R. China

[b] University of Chinese Academy of Sciences, Beijing 100049, P. R. China

[c] School of Materials Science and Engineering, South China University of Technology, Guangzhou 510640, P. R. China.

Corresponding authors

Nianqing Fu (N. Fu), E-mail: msnqfu@scut.edu.cn

Yuan Lin (Y. Lin), E-mail: linyuan@iccas.ac.cn

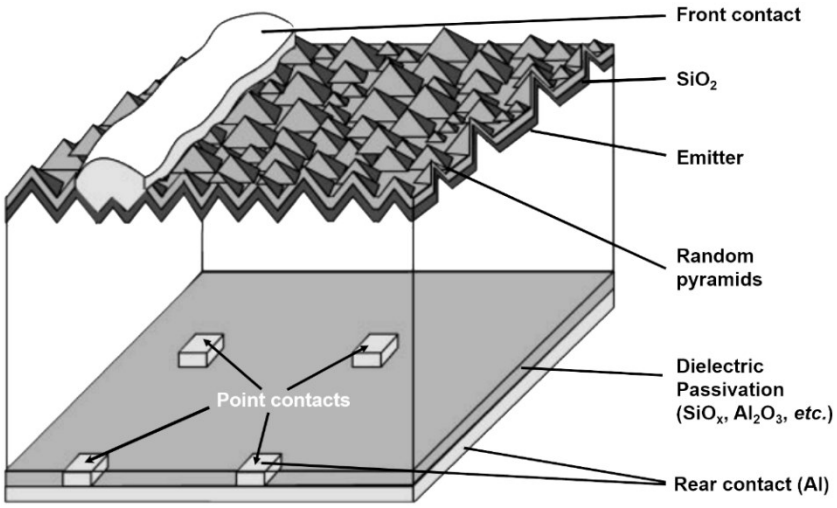

Fig. S1 Passivated and rear cell (PERC) structure most commonly used in high-efficiency Si solar cells.[S1,S2] The dielectric layer (SiO_x, Al_2O_3, SiN_x) inserted between the rear contact electrode and *p*-Si active layer is explored for surface passivation, while the point contacts decrease contact area and act as a way of reducing contact recombination.

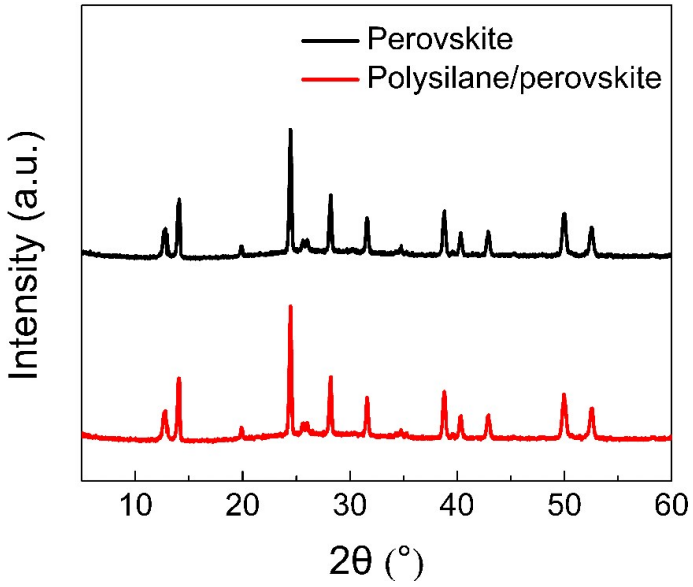

Fig. S2 XRD patterns of the perovskite and polysilane/perovskite films. The similar diffraction peaks in the two patterns indicate that 1) the deposition of polysilane by the solution process does not affect the crystalline structure of the underneath perovskite and 2) the deposited polysilane layer is thin and amorphous.

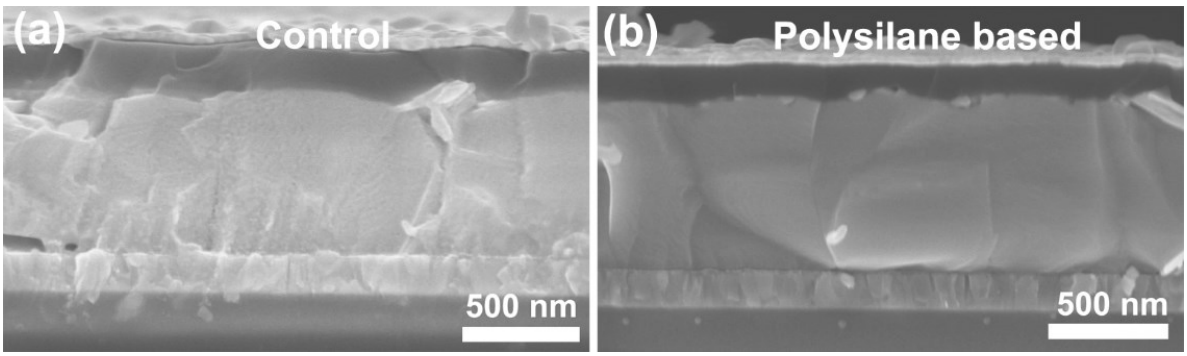

Fig. S3 Section-view SEM images of PSCs based on bare perovskite and polysilane/perovskite. A more obvious and sharp interface is observed for the device with a polysilane film is inserted between perovskite and HTL layers, thereby, protecting the integrity of each layer and improving the performance of the device.

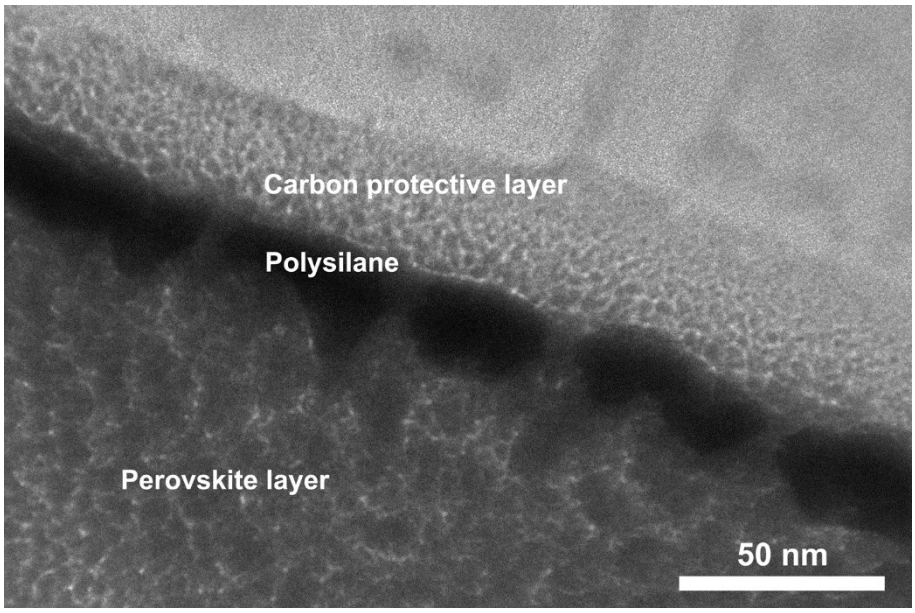

Fig. S4 cross-section view TEM image of the polysilane/perovskite bilayer showing the discontinuous polysilane films with reserved discrete holes. The carbon layer is deposited to prevent the polysilane/perovskite film from damaged by the FIB.

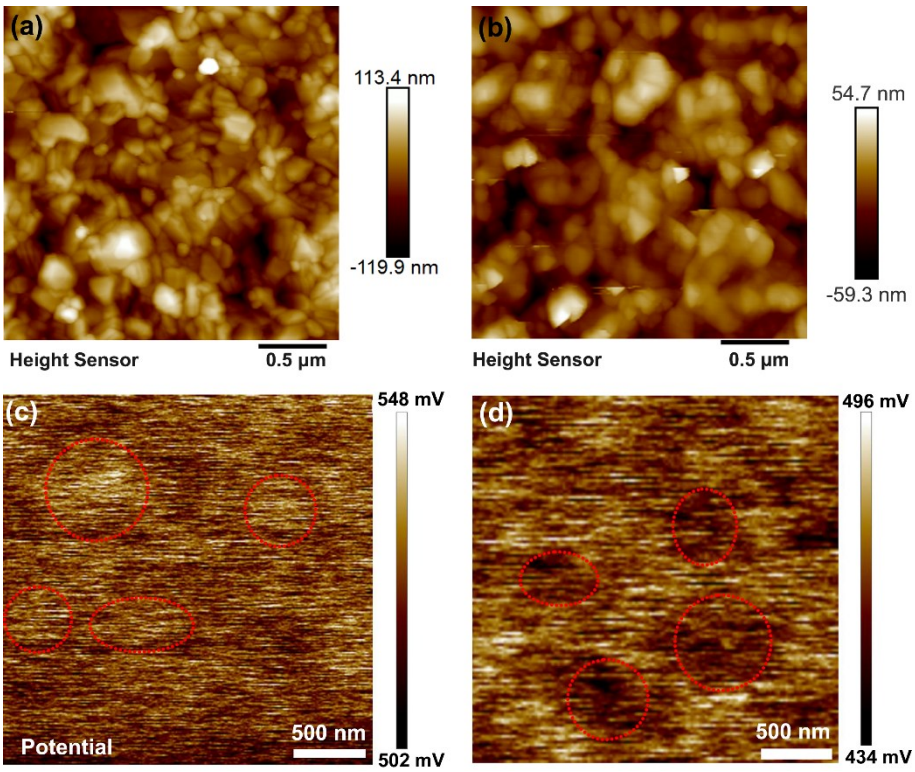

Fig. S5 (a, b) AFM morphologies and (c, d) KPFM potential distribution of the bare perovskite (left panels) and polysilane/perovskite (left panels) films.

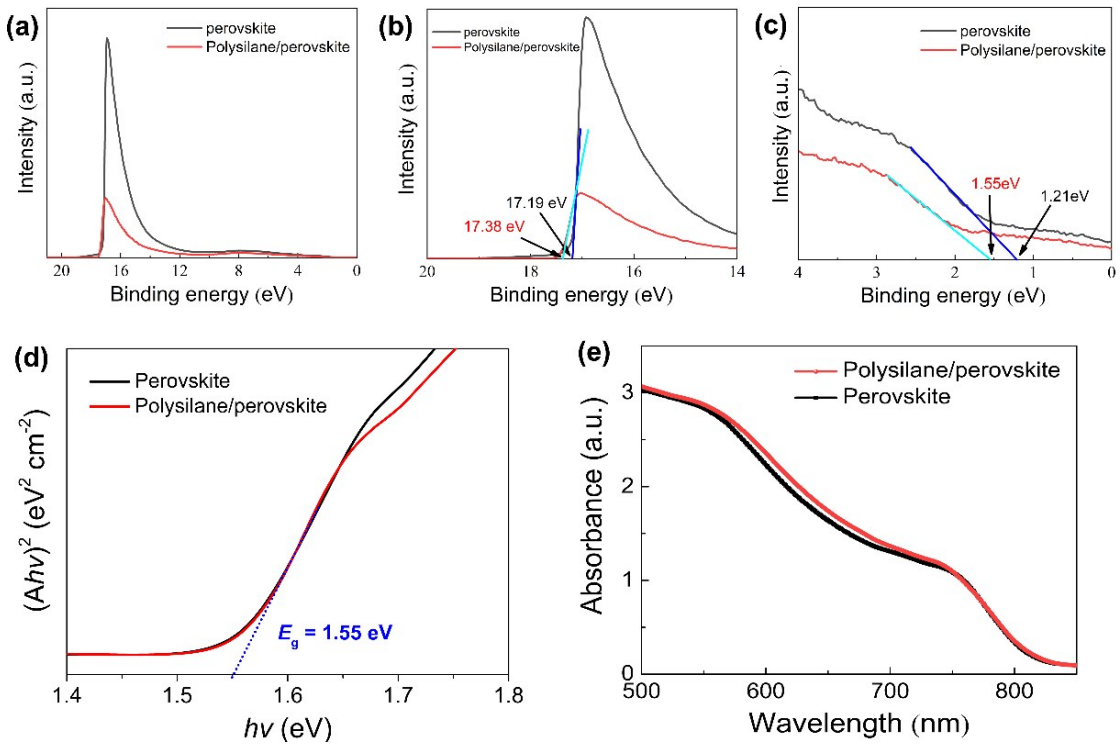

Fig. S6 UPS spectra showing the (a) full spectra, (b) cutoff regions, and (c) onset regions of pristine perovskite and polysilane/perovskite films. (d) Tauc plots and (e) UV-Vis absorption spectra of pristine perovskite and polysilane/perovskite films.

Fig. S5a-5c display the full spectra, cut-off region, and valence band region of the pristine perovskite and polysilane/perovskite films, respectively. As shown in Fig. S5b, the cutoff energy levels (E_{cutoff}) of pristine perovskite and polysilane/perovskite films are tested to be 17.19 eV and 17.38 eV, respectively. The Fermi levels (E_f) are thereby calculated to be -4.03 eV and -3.84 eV for pristine perovskite and polysilane/perovskite films, respectively, according to the relation of $E_f = E_{cutoff}$ - 21.22 eV. Based on the onset energy levels (E_{onset}) shown in Fig. S5c, the E_{VBM} (valance band maximum) is calculated to be -5.24 eV and -5.39 eV for pristine perovskite and polysilane/perovskite films, respectively, by employing the equation of $E_{VBM} = E_f - E_{onset}$. The energy bandgap ($E_g$) of pristine perovskite and polysilane/perovskite films can be obtained based on Tauc plots (Fig. S5d) that evolved from the UV-Vis absorbance of the two films (Fig. S5f). It is clear from the Tauc plots that the E_g remains unchanged after the polysilane coating, with a similar value of 1.55 eV. Based on the relation of $E_{CBM} = E_{VBM} + E_g$, the conduction band minimum (E_{CBM}) are determined to be -3.69 and -3.84 eV for pristine perovskite and polysilane/perovskite films, respectively. The slight downshift (0.15 eV) of both E_{CBM} and E_{VBM} after polysilane coating will not affect the charge transfer, in the point view of band alignment.

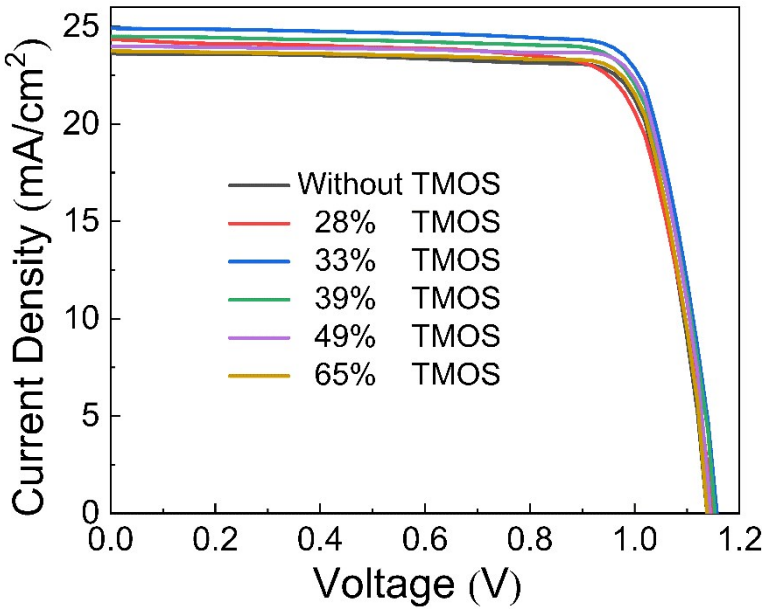

Fig. S7 Photocurrent-voltage curves of the control PSC and the PCRR devices that contain polysilane film derived from TMOS solution with various concentrations.

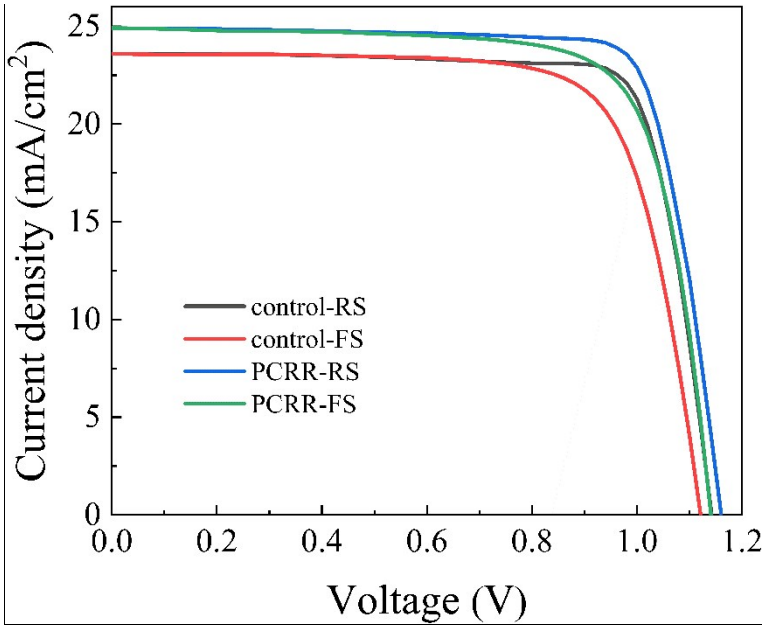

Fig. S8 Photocurrent-voltage curves of the control PSC and the PCRR device containing a polysilane film with optimal thickness. The results show an alleviated hysteretic behavior of PCRR-based PSCs.

Tbale S1 Photovoltaic parameters extracted from Fig. S7 and the hysteresis index calculated according to the relation of HI = ($PCE_{reverse}$ - PCE_{foward})/$PCE_{reverse}$×100%.

Devices	Scanning mode	V_{oc} (V)	J_{sc} (mA cm^{-2})	*FF*	PCE (%)	HI index (%)
Control	Reverse	1.138	23.59	77.89	20.91	5.35%
	Foward	1.121	23.60	74.83	19.79	
PCRR	Reverse	1.157	24.92	77.53	22.35	3.94%
	Foward	1.141	24.95	75.42	21.47	

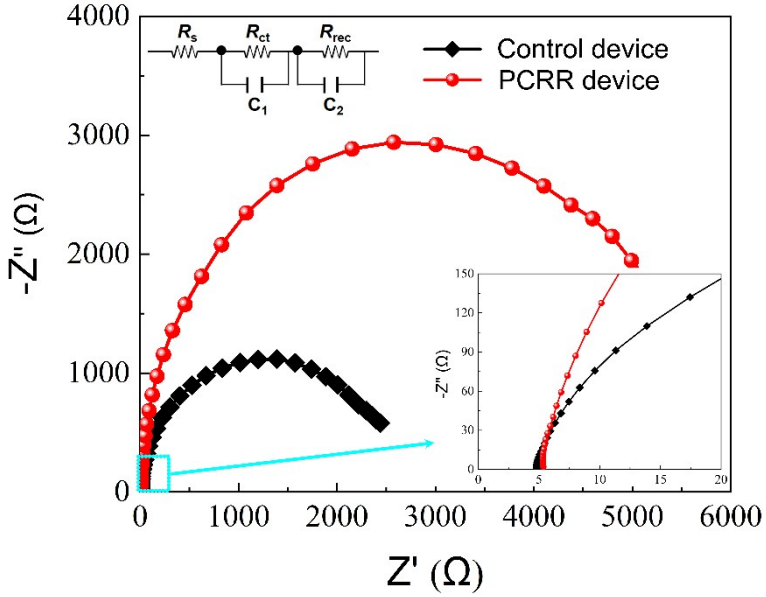

Fig. S9 The Nyquist plots of PSCs based on pristine perovskite and polysilane/perovskite films. The insert shows the enlargement of the high-frequency region and the equivalent circuit model employed to fit the Nyquist plots.

Table S2 The tr-PL parameters extracted from Fig. 5b, fitted by bi-exponential function of $y = y_0+A_1exp(-t/\tau_1) + A_2exp(-t/\tau_2)$.

Devices	$\mathbf{A_1}$	$\boldsymbol{\tau_1}$ **[ns]**	$\mathbf{A_2}$	$\boldsymbol{\tau_2}$ **[ns]**	$\boldsymbol{\tau_{ave}}$
Control	0.300	106.6	0.872	580.9	548.4
PCRR [33% TMOS]	0.146	170.9	0.895	952.3	929.7

Reference

s1 J. Schmidt, A. Merkle, R. Brendel, B. Hoex, M. C. M. van de Sanden and W. M. M. Kessels, *Prog. Photovoltaics*, 2008, **16**, 461-466.

s2 E. Schneiderlochner, R. Preu, R. Ludemann and S. W. Glunz, *Prog. Photovoltaics*, 2002, **10**, 29-34.